Equivalent pin-forces or equivalent moments for the modelling of piezoelectric patches: a parametric study

Taha Ajnada, Romain Corcolle, Yves Bernard, Laurent Daniel

Equivalent pin-forces or equivalent moments for the modelling of piezoelectric patches: a parametric study

Taha Ajnada[1,2], Romain Corcolle[3], Yves Bernard[1,2] and Laurent Daniel[1,2]

***Abstract*—**

Many piezoelectric (PZ) actuation or sensing systems consist of PZ patches bonded on elastic beams or blades.

In order to optimise the design of such systems, Finite Element Analysis (FEA) can be used. However, this option is relatively time consuming and not necessarily appropriate to the first steps of the design process.

The replacement of FEA by simple analytical tools is desirable in the early design stages in order to explore the optimal configurations for the device (beam dimensions, patch position and properties).

Two main modelling approaches can be found in the literature, based on the Solid Mechanics beam theory.
The first approach consists in replacing the PZ patch by two opposite forces positioned at the surface of the beam, each at one extremity of the PZ patch.
The second approach consists in replacing the PZ patch by two opposite moments positioned at the neutral axis of the beam, each at one extremity of the PZ patch.

The object of this paper is to detail these options, and to evaluate their range of validity. For this purpose, a parametric study is conducted on a cantilever beam structure to compare the different approaches for standard dimensions and material properties.

The results of corresponding FEA simulations are taken as reference. It is shown that the validity of analytical models is restricted to a narrow range of material properties and dimensions. This range is chosen when the error between the normalised displacements obtained analytically and those obtained by numerical calculation does not exceed 6%. Within this range, the two-moment model is revealed a more precise choice than two pin-forces. As a consequence, its validity range is larger compared to other analytical approaches. This is due to the introduction of the flexural stiffness of the PZ patch and of a realistic strain profile across the section of the structure. These results can be used to obtain analytical expressions of stress and strains in PZ actuation and sensing devices.

keywords: PZT, beam theory, PZ patch, cantilever, finite element modelling, equivalent models

[1]Université Paris-Saclay, CentraleSupélec, CNRS, Laboratoire de Génie Electrique et Electronique de Paris, 91192, Gif-sur-Yvette, France

[2]Sorbonne Université, CNRS, Laboratoire de Génie Electrique et Electronique de Paris, 75252, Paris, France

[3]Division of Engineering and Computer Science, NYU Shanghai, 1555 Century Avenue, Shanghai, 200122, People's Republic of China

NOMENCLATURE

E_b	Young modulus of beam material
s_{11}^E	Elastic compliance under constant electric field of PZ material along x-direction
E_p	Young modulus of PZ material along x-direction $\left(E_p = 1/s_{11}^E\right)$
l_b	Lenght of the beam
l_p	Lenght of the patch
b	Width of beam and patch (identical values)
t_b	Thickness of the beam
t_p	Thickness of the PZ patch
δ	Beam's free end displacement
ε_b	Strain across the beam section
ε_p	Strain across the PZ section
I_b	Quadratic moment of the beam $\left(I_b = bt_b^3/12\right)$
d_{31}	Transverse PZ constant of PZ material
V_0	Applied voltage
Λ	Stress-free PZ strain of the PZ patch along the x-direction $(\Lambda = d_{31}V_0/t_p)$

I INTRODUCTION

PZ materials are used in many actuation, sensing or transduction systems such as bistable MEMS ([1]), MEMS micro-valves ([2]), micropumps for drug delivery ([3], vibration energy harvesters ([4]), fuel injectors ([5]), haptic devices ([6]) or textile sensors ([7]), and their advantages are many.

First of all, response times are short. The materials can therefore be exploited at high frequencies (up to MHz ([8])). It is the property that is exploited, for example, in the case of fuel injection in automotive industry. It also means that a wide range of speeds can be exploited.

The stress levels that the materials can withstand are high ([9]). This makes it possible, for example, to generate high forces or torques in complete and compact systems that incorporate PZ materials.

Electromechanical conversion is intrinsic and it is simple to generate the electric field necessary for the conversion. This leads to compact and lightweight devices with simple structures ([10]). The above statement, combined with the exploitable speeds and stress levels, creates space for devices with high power-to-weight ratio.

The use of PZ materials, e.g. in travelling wave motors, leads to actuators with low rotational speeds ([11]). This property eliminates the need to use gearboxes for high torque and low speed applications.

The small displacements generated (under high voltage levels) lead to good controllability of the actuators and high

resolution, reaching the nanoscale ([12]), with very fast response times, below $1ms$.
The electromechanical conversion is increasingly improved ([13]). It takes place silently and with a negligible magnetic field (compared to conventional solutions).
Operation at cryogenic temperatures is possible even if the performance of the actuators is lower at low temperatures. PZ materials can operate at high temperatures without failure. Their usage temperature range is though limited by their Curie point T_C, about $160°C - 350°C$ for ferroelectric ceramics ([14]). The lifetime of these materials is relatively high, with very low consumption, especially in static use.
Finally, the use of PZ materials under vacuum or in clean rooms is permitted due to their composition ([15]).

In many applications, the PZ material is a patch bonded on a structure. The working principle of the device then relies on the interaction between the PZ patch and the structure (actuation, sensing or both).
In order to model the action of a PZ patch bonded on an elastic structure, several approaches are available. A variational formulation, combined to the coupled constitutive relations of PZ materials, can be used ([16], [17]). The problem cannot usually be solved analytically, and the implementation of a numerical model is required.
With the objective of establishing analytical relationships, [18] modelled the action of symmetrical bonded patches on an elastic structure, by using two equivalent pin-force, tangent to the surface of the structure. Alternately, [19] or [20] modelled the action of a PZ patch by two opposite moments, applied at the location of the patch extremities on the elastic structure.
There are also other models for predicting the system (substrate + actuator) response for thin and thick structures. We mention three of them in the following. First, the consistent plate model ([21]) that formulates the strain energy relations for a laminated plate, under the assumptions of thin and classical laminated plate theory. Second, the strain energy model ([22]) that models laminate beams and plates with attached or embedded finite length spatially-distributed induced strain actuators. Third, modes selective excitation ([23]) that predicts the behaviour of two dimensional patches of PZ material bonded to the surface of an elastic distributed structure and used as vibration actuators. Other works give an explicit analytical solution of deformation, vibration and optimal shape control of laminated cantilever PZ composite plates. The explicit formulation concerns the shape as a consequence of the applied loads, among others the PZ action. The resulting shape is then emphasised, rather than the causes (loads and more precisely the PZ action) that gave rise to it ([24], [25]).

The objective of this paper is to assess the range of validity of two main analytical approaches to model and give an explicit formulation of the effect of a PZ patch on an elastic beam. The first approach replaces the PZ patch by two equivalent opposite forces and the second by two equivalent opposite moments. A parametric evaluation is performed on a case study consisting of a PZ patch perfectly bonded to a cantilever beam structure.
In an experiment, the actuator is usually bonded to the structure via an adhesive.
The Physics of the electromechanical interaction between the piezoelectric element, the adhesive and the host structure is not yet been fully understood. Many fundamental problems related to its practical implementation have not been resolved. The proposed models need to be experimentally verified and improved ([26], [27]).
The experimental results show that increasing the adhesive thickness changes the electromechanical impedance and resonance frequency of the piezoelectric element, as well as the amplitude of the sensor signal ([28]).
For an actuator under the assumption of perfect bonding to the host structure, which is our study case, [18] showed that the shear stress between the actuator and the host beam was transferred mainly over an infinitesimal region at the actuator ends. This is consistent with the pin-forces and pin-moments models at the actuator ends that we have developed.
The corresponding Finite Element Analysis (FEA) is performed using COMSOL Multiphysics to serve as a reference solution for the problem.
Consistently with the studied analytical models, we consider in the FEA simulation that the system is without adhesive layer, i.e. the PZ actuator is perfectly bonded to the beam.
In our study, the direct solver implemented in Comsol Multiphysics MUMPS (MUltifrontal Massively Parallel sparse direct Solver) was used. MUMPS has the particularity to support cluster computing, allowing to use more memory than is typically available on a single machine.

In a first part, the study case is presented. The two analytical approaches are then presented and followed by the FEA implementation. A parametric study is then performed for different material and geometrical parameters. This allows defining the range of validity of the analytical models by comparison to FEA results.

II Study case

The considered problem (figure 1) consists in an elastic beam (e.g. steel), with length l_b and thickness t_b, clamped on its left side. The longitudinal linear elastic behaviour of the beam (along direction x) is characterised by the Young modulus E_b. A PZ patch (e.g. PZT), with length l_p and thickness t_p is bonded on the upper side of this cantilever beam. The PZ patch and the cantilever beam have the same width b. x_1 is the x-coordinate such that the patch is bonded to the beam on the zone $[x_1 \;\; x_1 + l_p]$. The Young modulus of the PZ patch along direction x is noted E_p. The PZ patch is equipped with electrodes on its upper and lower sides. V_0 is the voltage applied between these electrodes, the polarisation of the PZ patch being upward as shown in figure 1. The transverse PZ coefficient of the PZ patch is

denoted by d_{31}.

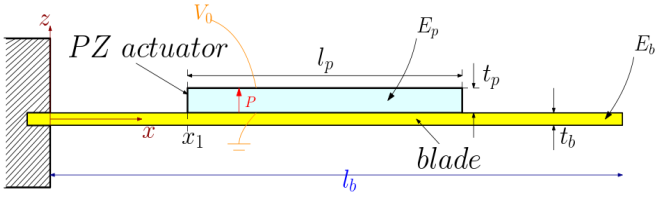

Fig. 1: *Case study of a PZ patch bonded to an elastic cantilever beam: geometric and material parameters.*

The PZ patch is excited by the application of a voltage along its polarisation direction z (Figure 1). Under free boundary conditions, the patch strains by the PZ deformation Λ, proportional to the applied voltage V_0. For a patch bounded on a blade, under plane stress assumption, the longitudinal strain ε_p in the patch is given by the behavioural law:

$$\varepsilon_p = \frac{\sigma_p}{E_p} + \Lambda \tag{1}$$

where Λ the stress-free PZ strain of the PZ patch along the x-direction:

$$\Lambda = \frac{d_{31} V_0}{t_p} \tag{2}$$

The different models (analytical and FEA) for this study case problem will be compared using the vertical displacement δ at the free (right) end of the cantilever beam. The longitudinal strain in the beam is noted ε_b. The assumption of plane stress is considered for the actuator and for the structure as well.

III Equivalent pin-force model([29], [30])

The pin-force model ([29], [30]) describes the action of the PZ patch on the beam by two opposite forces with module F, placed at the extremities of the PZ patch (figure 2).

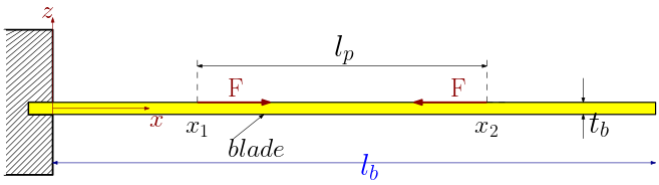

Fig. 2: *Simplification of the action of a PZ patch on an elastic structure using the pin-force model, case where the PZ stiffness is not considered.*

Several variants of the pin-force model can be obtained by following different assumptions. A first pin-force model can be developed assuming that the strain remains uniform throughout the section of the structure (figure 3). This assumption can be used when the structure is made of symmetrically bonded patches on each side of the beam.

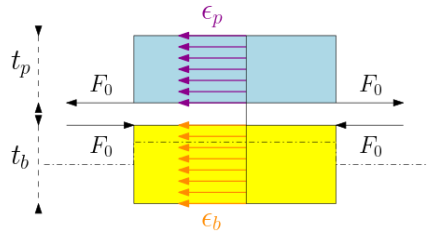

Fig. 3: *A first pin-force representation assuming uniform strain along the cross section of the beam and PZ patch ($\varepsilon_b = \varepsilon_p$).*

Although this assumption is obviously not relevant to describe the study case of figure 1 subjected to bending, the corresponding result is given below because it serves as a basis for more general configurations. In the absence of any external longitudinal force, the pin-force F_0 under uniform strain assumption, is given by (see ([29], [30])):

$$F_0 = -\frac{bE_b t_b}{1+\psi}\Lambda \tag{3}$$

with

$$\psi = \frac{E_b t_b}{E_p t_p} \tag{4}$$

Such model cannot describe bending, so that the obtained deflection δ is zero whatever the applied voltage.

A more refined pin-force model can be developed by maintaining the strain constant across the section of the PZ patch but assuming a linear variation of the strain across the section of the elastic beam (figure 4). In that case, the application of a voltage V_0 will result in a deflection δ.

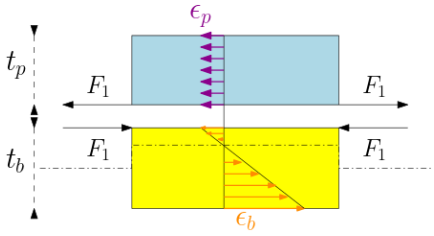

Fig. 4: *A pin-force representation assuming uniform strain along the cross section of the PZ patch and a linear variation of the strain along the cross section of the elastic beam.*

The pin-force F_1 in that case is given by (see ([29], [30])):

$$F_1 = -\frac{bE_b t_b}{3+\psi}\Lambda \tag{5}$$

In the construction of this model F_1, it should be mentioned that the stiffness added by the presence of the PZT patch is not taken into consideration.

A more precise pin-force model ([31]) can be obtained by adding the stiffness of the PZ patch to the stiffness of the structure, the resulting model is F_2 (figure 5).

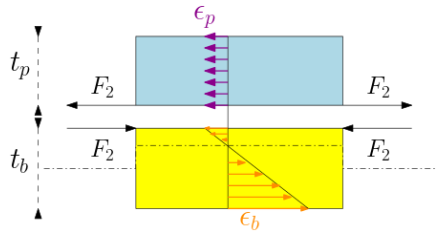

Fig. 5: *A pin-force representation assuming uniform strain along the cross section of the PZ patch and a linear variation of the strain along the cross section of the elastic beam. Actuator flexural stiffness is added to the model.*

The pin-force model F_2 in that case is given by (see Appendix B):

$$F_2 = -\frac{bE_b t_b}{3+\psi+\frac{t_p^2}{3t_b^2}}\Lambda \tag{6}$$

As mentioned in ([31]), the F_2 pin-force model contains some contradiction in it from a theoretical standpoint. By assuming a constant strain distribution in the actuator, we are in fact specifying that the actuator does not bend. However, the assumption of constant strain in the actuator seems acceptable, but neglecting the actuator flexural stiffness is what really leads to the discrepancy in the pin-force model for thin structures.

IV Equivalent two-moment model ([32])

The two-moment model in ([32]) describes the action of the PZ patch on the beam by two opposite moments with module M, placed at the extremities of the PZ patch (figure 6). By comparison to the previous two-force model, this model introduces a linear variation of the strain across the sections of both the elastic beam and the actuator.

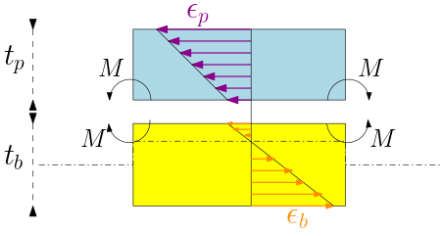

Fig. 6: *A two-moment representation assuming a linear variation of the strain along both the cross section of the elastic beam and PZ patch. Actuator flexural stiffness is included in the model.*

The extension and bending of the elastic beam is described by the strain field ε_b. This strain field can be written as the sum of a uniform strain (extension part) and a linearly varying strain (bending part). This strain can be seen as the result of the application of the two opposite moments. The moment M in that case is given by (see ([32])):

$$\frac{M}{bE_p} = \left(-K^f I_p + \left(K^e - 1 - z_n K^f\right) T - z_n \left(K^e - 1\right) t_p\right) \Lambda \tag{7}$$

where $I_p = \frac{\left(\frac{t_b}{2}+t_p\right)^3 - \left(\frac{t_b}{2}\right)^3}{3}$ and $T = \frac{\left(\frac{t_b}{2}+t_p\right)^2 - \left(\frac{t_b}{2}\right)^2}{2}$,
where z_n defines the neutral axis of the beam (z position for which the strain ε_b is zero):

$$z_n = \frac{E_p\left(t_p^2 + t_p t_b\right)}{2\left(E_b t_b + E_p t_p\right)} \tag{8}$$

and where

$$K^f = \frac{2}{t_b+t_p}\Big(1 - \frac{E_b E_p t_b^3 t_p + E_b^2 t_b^4 + E_p^2 t_p^4 + E_b E_p t_b t_p^3}{E_p^2 t_p^4 + E_b^2 t_b^4 + E_b E_p\left(4t_b^3 t_p + 6t_b^2 t_p^2 + 4t_b t_p^3\right)}\Big)$$

$$K^e = \frac{t_p^4 + \frac{E_b}{E_p} t_b^3 t_p}{t_p^4 + \frac{E_b^2}{E_p^2} t_b^4 + \frac{E_b}{E_p}\left(4t_b^3 t_p + 6t_b^2 t_p^2 + 4t_b t_p^3\right)}$$

are introduced to simplify the moment formula.

V Expression of the deflection in the study case

Equations (5) and (6) give the expressions for a pin-force model without considering the stiffness of the PZ patch ($F = F_1$) and with considering it ($F = F_2$), respectively. Equation (7) defines a two-moment model with the moments applied at the patch extremities. The modelling options for the modelling of a cantilever beam, taken as the reference study case, are illustrated in figure 7.

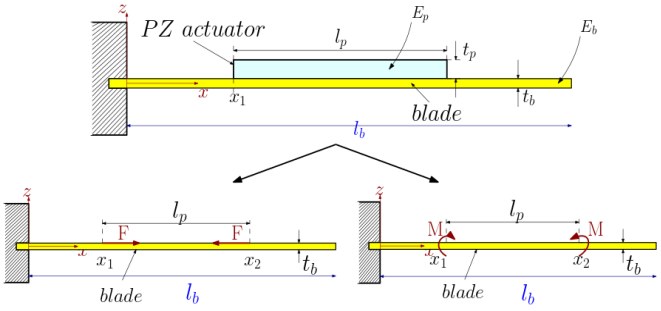

Fig. 7: *Two modelling options for a cantilever beam actuated by a PZ patch: pin-force (left) and two-moment (right) models.*

Using the standard Euler-Bernoulli theory, the expression of the transverse displacement $w(x)$ of the beam neutral axis (along z-direction) can be directly derived form the expressions of F_1, F_2 or M. The deflection δ at the free (right) end of the cantilever beam is then simply given by:

$$\delta = w(x = l_b) \tag{9}$$

This value δ will be used in the following as the comparison indicator between the different modelling approaches.

According to Euler-Bernoulli theory, the transverse displacement $w(x)$ must obey the following equation:

$$w'' = \frac{d^2w}{dx^2} = -\frac{M_{fz}}{(EI)} \tag{10}$$

M_{fz} is the bending moment of the beam and (EI) is the bending stiffness of the beam. It is defined as:

$$(EI) = E_b I_b \tag{11}$$

for the F_1 model, and as:

$$(EI) = E_b I_b + E_p I_p \tag{12}$$

for the F_2 and M models. The difference between these definitions comes from the fact that the bending stiffness of the PZ patch is not neglected in the two latter models. The definition of the bending moment M_{fz} naturally leads to consider three distinct areas on which the transverse displacement is defined. The expression of the transverse displacement $w(x)$ is given below according to the three considered approaches. It is noted $w_{F1}(x)$, $w_{F2}(x)$ and $w_M(x)$ for the F_1, F_2 and M models, respectively.

For $0 \leq x < x_1$:

$$w_{F1}(x) = w_{F2}(x) = w_M(x) = 0 \tag{13}$$

For $x_1 \leq x < x_2$:

$$\begin{cases} w_{F1}(x) = -\dfrac{F_1 t_b}{4E_b I_b}.(x-x_1)^2 \\ w_{F2}(x) = -\dfrac{F_2 t_b}{4\left(E_b I_b + E_p I_p\right)}.(x-x_1)^2 \\ w_M(x) = -\dfrac{M}{2\left(E_b I_b + E_p I_p\right)}.(x-x_1)^2 \end{cases} \tag{14}$$

For $x_2 \leq x \leq l_b$:

$$\begin{cases} w_{F1}(x) = -\dfrac{F_1 t_b}{2E_b I_b}.(x_2-x_1).x \\ \qquad + \dfrac{F_1 t_b}{4E_b I_b}.(x_2^2-x_1^2) \\ w_{F2}(x) = -\dfrac{F_2 t_b}{2\left(E_b I_b + E_p I_p\right)}.(x_2-x_1).x \\ \qquad + \dfrac{F_2 t_b}{4\left(E_b I_b + E_p I_p\right)}.(x_2^2-x_1^2) \\ w_M(x) = -\dfrac{M}{E_b I_b + E_p I_p}.(x_2-x_1).x \\ \qquad + \dfrac{M}{2\left(E_b I_b + E_p I_p\right)}.(x_2^2-x_1^2) \end{cases} \tag{15}$$

The deflection δ_{F1}, δ_{F2} and δ_M for the F_1, F_2 and M models, respectively, can then be easily obtained at the position $x = l_b$:

$$\begin{cases} \delta_{F1} = w_{F1}(l_b) = -\dfrac{F_1 t_b}{2E_b I_b}.(x_2-x_1).l_b \\ \qquad + \dfrac{F_1 t_b}{4E_b I_b}.(x_2^2-x_1^2) \\ \delta_{F2} = w_{F2}(l_b) = -\dfrac{F_2 t_b}{2\left(E_b I_b + E_p I_p\right)}.(x_2-x_1).l_b \\ \qquad + \dfrac{F_2 t_b}{4\left(E_b I_b + E_p I_p\right)}.(x_2^2-x_1^2) \\ \delta_M = w_M(l_b) = -\dfrac{M}{E_b I_b + E_p I_p}.(x_2-x_1).l_b \\ \qquad + \dfrac{M}{2\left(E_b I_b + E_p I_p\right)}.(x_2^2-x_1^2) \end{cases} \tag{16}$$

It can be noticed that all models give a similar form for the expression of the deflection δ so that equation (16) can be re-written as follows:

$$\begin{cases} \delta_{F1} = K.\dfrac{1}{3+\widetilde{E}.\widetilde{T}} \\ \delta_{F2} = K.\dfrac{1}{3+\widetilde{E}.\widetilde{T}+\frac{1}{3\widetilde{T}^2}} \\ \delta_M = K.\dfrac{\widetilde{T}(1+\widetilde{T})}{\widetilde{E}.\widetilde{T}^3+4\widetilde{T}^2+6\widetilde{T}+4+\widetilde{E}} \end{cases} \tag{17}$$

where

$$K = \frac{6d_{31}V_0}{t_b t_p} l_b l_p \left(1 - \frac{l_p}{2l_b} - \frac{x_1}{l_b}\right) \tag{18}$$

and $\widetilde{T} = \frac{t_b}{t_p}$ and $\widetilde{E} = \frac{E_b}{E_p}$ are dimensionless parameters characteristic of the structure geometry and material choice, respectively.

Comparing the three analytical models then reduces to comparing the dimensionless functions f_{F1}, f_{F2}, f_M, defined by equation (19):

$$\begin{cases} f_{F1}(\widetilde{T},\widetilde{E}) = \dfrac{1}{3+\widetilde{E}.\widetilde{T}} \\ f_{F2}(\widetilde{T},\widetilde{E}) = \dfrac{1}{3+\widetilde{E}.\widetilde{T}+\frac{1}{3\widetilde{T}^2}} \\ f_M(\widetilde{T},\widetilde{E}) = \dfrac{\widetilde{T}(1+\widetilde{T})}{\widetilde{E}.\widetilde{T}^3+4\widetilde{T}^2+6\widetilde{T}+4+\widetilde{E}} \end{cases} \tag{19}$$

It is then evident that, if the deflection δ in the cantilever beam problem is taken as the comparison indicator, the difference between the three approaches only depends on the dimensionless parameters $\widetilde{T}$ and $\widetilde{E}$, namely the ratio of the thicknesses and the ratio of the Young modulus of the elastic beam and PZ patch. The functions $f(\widetilde{T},\widetilde{E})$ will be named "normalised deflections" in the following.

It can also be noticed that all analytical models provide a very similar equation for $w(x)$, namely a horizontal line between 0 and x_1, a parabolic function between x_1 and x_2 and again a straight line between x_2 and l_b. Since the continuity of the derivative of $w(x)$ is imposed, the equation $w(x)$ is actually fully defined by $\delta = w(l_b)$ and the geometric

parameters:
For $0 \leq x < x_1$:

$$w_{F1}(x) = w_{F2}(x) = w_M(x) = w_\delta(x) = 0 \tag{20}$$

For $x_1 \leq x < x_2$:

$$\begin{aligned} w_{F1}(x) = w_{F2}(x) = w_M(x) = w_\delta(x) \\ = -\frac{\delta}{x_2 - x_1} . \frac{1}{x_2 + x_1 - 2l_b} . (x - x_1)^2 \end{aligned} \tag{21}$$

For $x_2 \leq x \leq l_b$:

$$\begin{aligned} w_{F1}(x) = w_{F2}(x) = w_M(x) = w_\delta(x) \\ = \frac{\delta}{x_2 + x_1 - 2l_b} . (x_2 + x_1 - 2x) \end{aligned} \tag{22}$$

For a given deflection, the deformation of the beam is therefore the same for all models.
The problem being purely elastic, the deformation of the beam provides the internal stress. Therefore, if the tip deflection is the same for two models, the deformed shape is also the same, as well as the internal stresses. This is the reason why the tip deflection of the beam has been chosen as a convenient comparison indicator.

VI Parametric study

The normalised deflections f have been calculated for the three analytical models of interest for different thickness ratios $\widetilde{T}$ varying from 0.1 to 10, and for different Young modulus ratios $\widetilde{E}$ varying from 0.1 to 5.
The results obtained with the three models for the normalised deflections f are presented in figure 8.

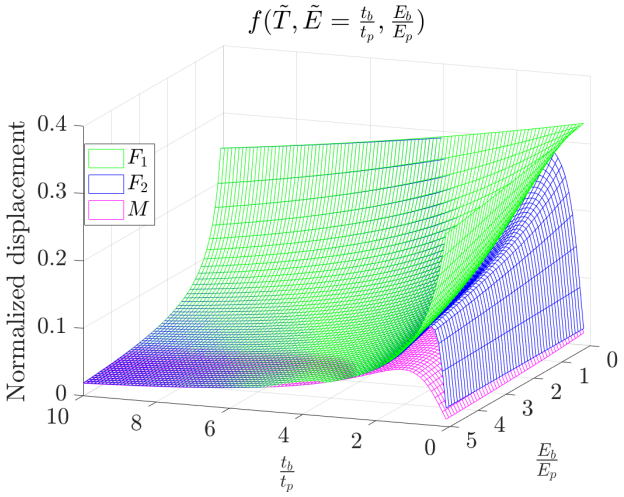

Fig. 8: *Comparison of the pin-force (F_1 and F_2) and two-moment (M) models for the normalised deflection f in the cantilever beam reference problem.*

For thickness ratios $\widetilde{T} \leq 2$, the responses are significantly different between the three models, with relative errors of more than 30% on average, regardless of Young modulus ratio $\widetilde{E}$. For $\widetilde{T} \geq 2$, F_1 and F_2 models are close but remain different from the results of the two-moment model. Finally, on the area defined by $\widetilde{T} \geq 4$ and $\widetilde{E} \geq 2$, the three analytical approaches provide very similar results, with relative errors of less than 6%, so that they could be indifferently used in that range of parameters.

VII Validation using FEA

The analytical approaches state that the normalized displacement only depends on $\widetilde{T}$ and $\widetilde{E}$, the thickness and Young modulus ratios of the beam and the PZ patch. This result is tested using a FEA simulation that will provide a reference solution. In agreement with the analytical models, the FEA study is implemented under the assumption of plane stress. Regarding the FEA simulations, the dimensions and material parameters have been set as follows. The PZ material under consideration is PZT so that the transverse PZ coefficient d_{31} is 62.10^{-12} m/V and the Young modulus E_p is 81 GPa, which are typical values for PZT [1]. The range of exploration for the dimensionless parameter $\widetilde{E}$ has been set to {0.1 to 5}. The beam Young modulus is defined by $E_p.\widetilde{E}$ and ranges from 8 GPa to 405 GPa. This wide range includes typical values for steel or aluminium. For the thickness of the PZ patch, it has been considered in the range {0.1 mm to 3.1 mm}, which corresponds to typical commercially available thicknesses for PZT patches. The range of exploration for the dimensionless parameter $\widetilde{T}$ has been set to {0.1 to 10}. This choice covers thicknesses for the beam from 0.01 mm to 30 mm. All other parameters have been given fixed values. The set of parameters used for the FEA simulations are summarised in table I.

For each FEA simulation, the normalised deflection f_{FEA} is obtained by dividing the deflection δ by the parameter K defined by equation (18). Then, for each value of t_p, the normalised deflection is plotted against $\widetilde{T}$ and $\widetilde{E}$.

Parameter	Unit	Value
PZ		
E_p	GPa	81
t_p	mm	[0.1 : 0.3 : 3.1]
l_p	mm	10
b	mm	10
d_{31}	m/V	62.10^{-12}
Voltage V_0	V	100
Position x_1	mm	10
Beam		
E_b	GPa	$E_p.\widetilde{E}$
t_b	mm	$t_p.\widetilde{T}$
l_b	mm	40
b	mm	10
Parameter ratios		
$\widetilde{E}$	-	[0.1 : 0.5 : 5]
$\widetilde{T}$	-	[0.1 : 0.5 : 10]

TABLE I: *Dimensions and material parameters used for the FEA simulation of the cantilever beam case study.*

Figure 9 shows the ($\widetilde{T}$,$\widetilde{E}$,f_{FEA}) plot for the two extreme values of t_p. All intermediate calculations are positioned evenly between the two extreme curves. A third curve of

[1] http://www.noliac.com/

the average between the two is then plotted. We first notice that the obtained trends are consistent with figure 8.

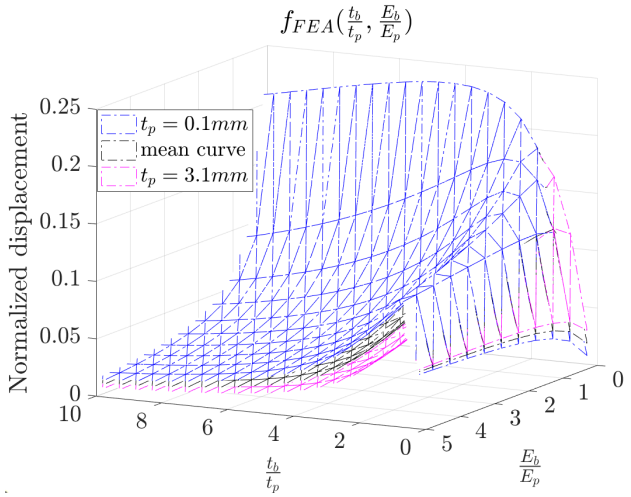

Fig. 9: *3D FEA results of the normalised deflection f_{FEA} for different PZT thicknesses t_p.*

From figure 9, it is clear that the normalised deflection is not only a function of the dimensionless ratios $\widetilde{T}$ and $\widetilde{E}$, as stated by the analytical approaches, but is also affected by the thickness of the patch.

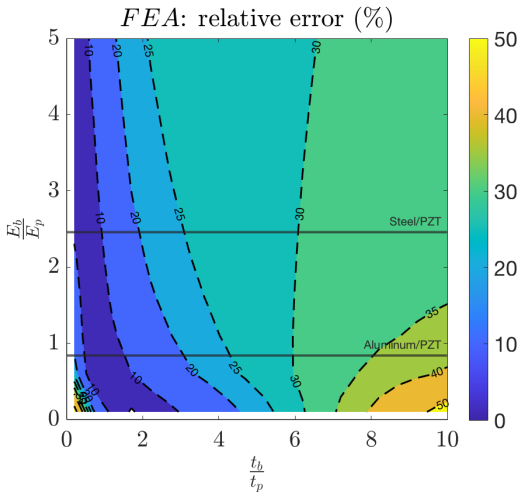

Fig. 10: *Relative error between ($\frac{t_b}{t_p}$,$\frac{E_b}{E_p}$,f_{FEA}) two extreme curves, isobase map. Light yellow denotes values greater than or equal to 50%. The two horizontal lines are corresponding to $\widetilde{E}$ of the steel and aluminium association with PZT.*

Figure 10 shows the relative error (defined as $|f_{(FEA,0.1)} - f_{(FEA,3.1)}|/f_{(FEA,3.1)}$ between the two extreme curves ($tp = 0.1$ *mm* and $tp = 3.1$ *mm*). This leads to define an error threshold, below which this assumption is considered valid. We propose, according to the error map and isovalues, that for a relative error below 20%, the normalised deflection will be considered as correctly defined by the parameter ratios. The comparison between the analytical models and the FEA model will only be investigated in this range of parameter variation. Outside this range, even in the case where the error between the analytical models and the FEA model is relatively small, nothing can be concluded.

The statement of depending only on parameter ratios is not restricted to a specific area in the analytical case, unlike the FEA model. The reason behind this lies in the simplifying assumptions of the analytical model: bringing the action of the patch to a point of application, simplifying the behaviour law of the PZ material to only isotropic and x-axis behaviour, while the FEA model takes into account all components of the coupling and compliance matrices of the PZT.

The 2D FEA simulations are now compared to analytical results. The reference result f_{FEA} is chosen to be the extreme two curves from figure 9. Relative error is then defined by the maximum of the error between the value of the analytical normalised displacement f_{anal}: (f_{F1}, f_{F2} or f_M) and the value of the FEA normalised displacement on one of the extreme curves $f_{(FEA,3.1)}$ or $f_{(FEA,0.1)}$:

$$max\left(\frac{|f_{anal} - f_{(FEA,3.1)}|}{f_{(FEA,3.1)}}, \frac{|f_{anal} - f_{(FEA,0.1)}|}{f_{(FEA,0.1)}}\right).$$

Error maps of the three analytical models (f_{F1}, f_{F2}, f_M) with respect to that reference are presented in the following figures.

It is reminded that the analytical model validity is investigated only in the region where the definition of the normalised deflection f as a function of only ratios $\widetilde{T}$ and $\widetilde{E}$ is considered valid. This range has been reported from figure 10 on all figures with dashed red isovalues.

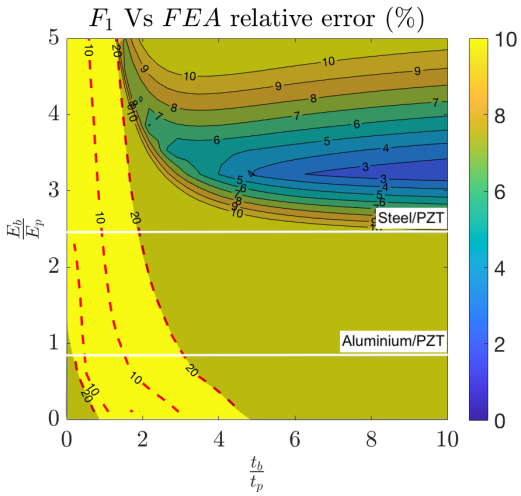

Fig. 11: *Relative error between the F_1 pin-force model and the FEA solution taken as reference. Range delimited by dotted red lines: all models assume the same statement (dependence only on $\frac{t_b}{t_p}$ and $\frac{E_b}{E_p}$). A mask is added outside the domain validated by FEA. The two horizontal lines are corresponding to $\widetilde{E}$ of the steel and aluminium association with PZT.*

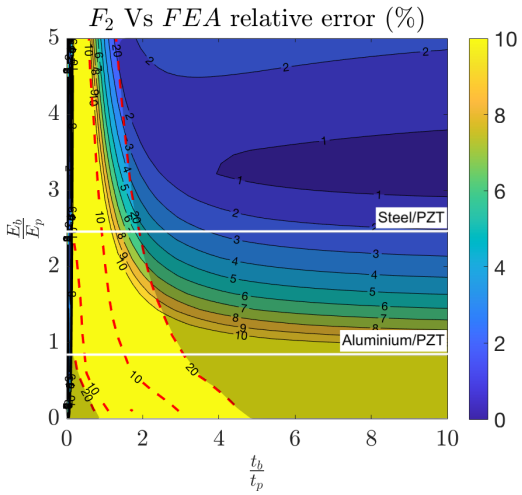

Fig. 12: *Relative error between the F_2 pin-force model and the FEA solution taken as reference. Range delimited by dotted red lines: all models assume the same statement (dependence only on $\frac{t_b}{t_p}$ and $\frac{E_b}{E_p}$). A mask is added outside the domain validated by FEA. The two horizontal lines are corresponding to $\widetilde{E}$ of the steel and aluminium association with PZT.*

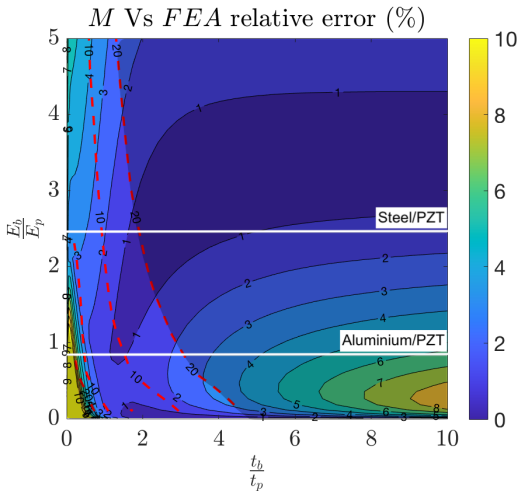

Fig. 13: *Relative error between the M pin-moment model and the FEA solution taken as reference. Range delimited by dotted red lines: all models assume the same statement (dependence only on $\frac{t_b}{t_p}$ and $\frac{E_b}{E_p}$). A mask is added outside the domain validated by FEA. The two horizontal lines are corresponding to $\widetilde{E}$ of the steel and aluminium association with PZT.*

In order to allow a clearer comparison between the three analytical models, all colour maps have been saturated above error values of 10%. A value of 10% (yellow) designates an error equal or higher than 10%.

The inaccuracy of the F_1 model is very high as shown in figure 11. In the investigation zone, the error between the analytical F_1 model and FEA model is always higher than 10%.

The F_2 model is slightly better as shown in figure 12. For $\widetilde{T} \geq 1$ and $\widetilde{E} \geq 2$ in the investigation zone, the relative error generally remains less than 6%.

The M model, associated to less drastic assumptions, logically shows the best results (see figure 13). In the full range tested for the two dimensionless parameters $\widetilde{T}$ and $\widetilde{E}$, in the investigation zone, the relative error does not exceed 3% in a large part of the investigation zone, and stays below 6% almost everywhere.

To summarise the analysis performed this paper, figure 14 shows the areas of validity of the analytical models F_1, F_2 and M, based on the FEA results.

Taking into account classical beam materials: steel and aluminium, we can highlight the following findings.

F_1 model is not applicable for either the Steel-PZT or Aluminium-PZT combination. It cannot be used either for other types of materials based on the FEA result.

F_2 model can be used for a Steel-PZT combination in a very narrow range of thickness ratios (around $\widetilde{T} = 2$).

By contrast, M model can be applied to both steel and aluminium cases. The only requirement is that the condition on the investigation zone, validated by FEA, is respected. This concerns ratios $0.1 \leq \widetilde{T} \leq 2$ for steel beam and $0.5 \leq \widetilde{T} \leq 3$ for aluminium beam.

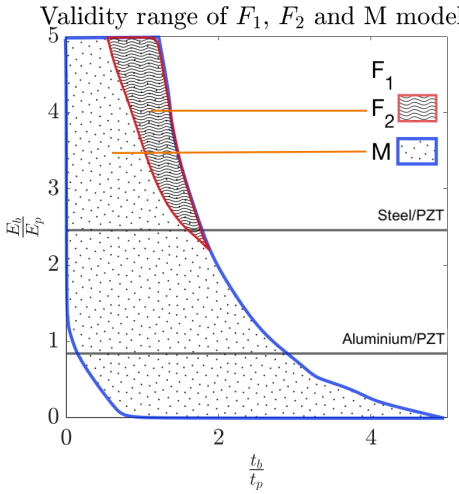

Fig. 14: *Conclusion on the validity domains of the three analytical models, with respect to the FEA calculation.*

VIII Conclusions

After the analysis carried out in this work, the following conclusions can be drawn:

1) Several approaches can be built depending on the assumptions made on the variation of the strain across the cross-section of the beam and the actuator. Three options were retained and named F_1, F_2 and M-model.
2) The comparison between these models can be summarised to a function of dimensionless parameters: thicknesses and Young modulus ratios.

However, FEA results showed that the action of a PZT can be accurately modelled by such a function only in a given range of dimensionless parameters.

3) Three dimension plots and error maps of analytical and numeric models show shortcomings with respect to the relevance of the F_1 model, which is by construction very simple and is based on many simplifying assumptions.
4) Pin-force model with uniform strain distribution on only the active element can be used in the case where the flexural stiffness of the actuator is added. This concerns the case where the thickness of the beam is 1 to 2 times larger than the PZ, and for many types of beam materials.
5) Moment model, which models the action of a PZ patch by two moments applied at its ends, has been defined as the best model. Its results are validated by comparing its prediction on deflection with the results obtained from the FEA study.

The key factors explaining the superiority of the M model is the introduction of the flexural stiffness of the PZ patch on one hand, and the introduction of a realistic variation of the strain across the cross-section of the structure, on the other hand.

It is believed that the conclusions obtained in this work on a simple structure can be extrapolated to more complex structures on which PZ patches are glued. However, the study dealt with the case of static excitation of the actuator. The dynamic case where the actuator is supplied with frequency voltage is a prospect for future work.

ACKNOWLEDGEMENT

This work is supported by the Automotive Mechatronics Chair, a cooperation between Faurecia, CentraleSupélec and Esigelec.

REFERENCES

[1] M.T.A. Saif. On a tunable bistable MEMS - theory and experiment. *Journal of Microelectromechanical Systems*, 9(2):157–170, 2000.

[2] I. Chakraborty, W.C. Tang, D.P. Bame, and T.K. Tang. MEMS microvalve for space applications. *Sensors and Actuators*, 83:188–193, 2000.

[3] C. Qifeng, L. Chengliang, and F.Z. Xuan. Study on a piezoelectric micropump for the controlled drug delivery system. *Microfluid Nanofluid*, 3:377–390, 2007.

[4] X. Wang, X. Liang, Z. Hao, H. Du, N. Zhang, and M. Qian. Comparison of electromagnetic and piezoelectric vibration energy harvesters with different interface circuits. *Mech. Syst. Signal Process*, 72-73:906–924, 2016.

[5] W. Yu, W. Yang, K. Tay, B. Mohan, F. Zhao, and Y. Zhang. Macroscopic spray characteristics of kerosene and diesel based on two different piezoelectric and solenoid injectors. *Experimental Thermal and Fluid Science*, 76:12–23, 2016.

[6] S. Ghenna, F. Giraud, C. Giraud-Audine, and M. Amberg. Vector control of piezoelectric transducers and ultrasonic actuators. *IEEE Transactions on Industrial Electronics*, PP(99):4880–4888, 2017.

[7] E. Nilsson, A. Lund, C. Jonasson, C. Johansson, and B. Hagstrom. Poling and characterization of piezoelectric polymer fibers for use in textile sensors. *Sensors and Actuators A: Physical*, 76:12–23, 2013.

[8] D. Zhang, B. Su, T. W. Button, A. Abrar, K.J. Kirk, and S. Cochran. Piezoelectric 1–3 Composites for High Frequency Ultrasonic Transducer Applications. *Ferroelectrics*, 304:1:201–205, 2004.

[9] A.J. Bell, T.P. Comyn, and T.J. Stevenson. Expanding the application space for piezoelectric materials. *APL Materials*, 9, 010901:1–6, 2021.

[10] P. Wiwattananon, O.K. Bergsma, and H. Bersee. Understanding piezoelectric composite–based actuators with nonlinear and 90° domain walls effects. *Journal of Intelligent Material Systems and Structures*, 27(13):1738–1754, 2015.

[11] S. Zhang, R. Xia, L. Lebrun, D. Anderson, and T.R. Shrout. Piezoelectric materials for high power, high temperature applications. *Materials Letters*, 59:3471–3475, 2005.

[12] Y.Y. Shi, C. Lou, and J. Zhang. Investigation on a linear piezoelectric actuator based on stick-slip/scan excitation. *Actuators 2021*, 10,39:1–12, 2021.

[13] S.C. Thompson, R.J. Meyer, and D.C. Markley. Performance of tonpilz transducers with segmented piezoelectric stacks using materials with high electromechanical coupling coefficient. *Acoustical Society of America*, 135(1):155–164, 2014.

[14] S. Zhang and F. Yu. Piezoelectric materials for high temperature sensors. *The American Ceramic Society*, 94:3153–3170, 2011.

[15] A.V. Shchagin, V.S. Miroshnik, V.I. Volkov, A.S. Kubankin, and O.O. Ivashchuk. Ceramic piezoelectric transformer in vacuum for acceleration of electrons and production of x-rays. *Acoustical Society of America*, 11, 1188:1–7, 2018.

[16] R. Corcolle, E. Salaün, F. Bouillault, Y. Bernard, C. Richard, A. Badel, and D. Guyomar. Modeling of a beam structure with piezoelectric materials: introduction to ssd techniques. *COMPEL*, 27(1):205–214, 2008.

[17] Biao Wang, Xiaowei Luo, Yizhong Liu, and Zhengbao Yang. Thickness-variable composite beams for vibration energy harvesting. *Composite Structures*, 244:112232, 2020.

[18] E.F. Crawley and J. De Luis. Use of piezoelectric actuators as elements of intelligent structures. *AIAA JOURNAL*, 25:1373–1385, 1987.

[19] V. Piefort and A. Premont. Finite element modelling of piezoelectric structures. *CiteSeerX*, 2001.

[20] E. Salaün, R. Corcolle, F. Bouillault, Y. Bernard, C. Richard, A. Badel, and D. Guyomar.

[21] E.F. Crawley and K.B. Lazarus. Induced strain actuation of isotropic and anisotropic plates. *AIAA Journal*, 29(6):944–951, 1989.

[22] B.T. Wang and C.A. Rogers. Modelling of finite length spatially distributed induced strain actuators for laminate beams and plates. *AIAA Journal*, 2(1):1511–1520, 1991.

[23] E.K. Dimitriadis, C.R. Fuller, and C.A. Rogers. Piezoelectric actuators for distributed vibration excitation of thin plates. *J. of Vibration and Acoustics*, 113(1):100–107, 1991.

[24] Soheil Gohari, S. Sharifi, and Zora Vrcelj. New explicit solution for static shape control of smart laminated cantilever piezo-composite-hybrid plates/beams under thermo-electro-mechanical loads using piezoelectric actuators. *Composite Structures*, 145:89–112, 2016.

[25] Soheil Gohari, F. Mozafari, N. Moslemi, Saeed Mouloodi, S. Sharifi, Hadi Rahmanpanah, and Colin Burvill. Analytical solution of the electro-mechanical flexural coupling between piezoelectric actuators and flexible-spring boundary structure in smart composite plates. *Archives of Civil and Mechanical Engineering*, 21(1):1–25, 2021.

[26] Y. G. Xu and G. R. Liu. A modified electro-mechanical impedance model of piezoelectric actuator-sensors for debonding detection of composite patches. *Journal of Intelligent Material Systems and Structures*, 13(6):389–396, 2002.

[27] Suresh Bhalla and Chee Kiong Soh. Electromechanical impedance modeling for adhesively bonded piezo-transducers. *Journal of Intelligent Material Systems and Structures*, 15(12):955–972, 2004.

[28] Xinlin P. Qing, Hian-Leng Chan, Shawn J. Beard, Teng K. Ooi, and Stephen A. Marotta. Effect of adhesive on the performance of piezoelectric elements used to monitor structural health. *International Journal of Adhesion and Adhesives*, 26(8):622–628, 2006.

[29] T. Bailey and J.E. Ubbard. Distributed piezoelectric-polymer active vibration control of a cantilever beam. *Journal of Guidance, Control, and Dynamics*, 8(5):605–611, 1985.

[30] E.F. Crawley and E.H. Anderson. Detailed Models of Piezoceramic Actuation of Beams. *Journal of Intelligent Material Systems and Structures*, 1(1):4–25, 1990.

[31] Z. Chaudhry and C.A. Rogers. The pin-force model revisited. *Journal of Intelligent Material Systems and Structures*, 5:347–354, 1994.

[32] G.P. Gibbs and C.R. Fuller. Excitation of thin beams using asymmetric piezoelectric actuators. *Acoustical Society of America*, 89:3221–3227, 1998.

=2